



The role of low frequency drift waves in driving non-classical transport in magnetic nozzles

Shadrach T. Hepner*

University of Michigan, Ann Arbor, MI, 48109

Benjamin A. Jorns†

University of Michigan, Ann Arbor, MI, 48109

2020 AIAA Propulsion Energy, AIAA-2020-3644

The presence of unstable modes is investigated in a magnetic nozzle. Electrostatic probes are used to characterize the steady state properties, and probe pairs biased negatively are used to measure wave propagation in three dimensions. The experiment is repeated for a low and high flow condition. An incoherent mode is observed in both conditions and determined to fit the description of a lower hybrid drift instability. A low frequency mode is also observed in the low flow case that forms an $m = 1$ mode downstream. It is theorized that this wave may be an anti drift instability. Anomalous collision frequencies are defined for each wave and discussed in the context of electron cross field transport and thruster performance. The incoherent mode is found to have a strong effect in both operating conditions in diverging the electron population, but is several orders of magnitude stronger in the low flow case. The influence of the low frequency mode appears to be significantly less than the incoherent mode under the anti drift instability theory. However, it is observed to propagate opposite of the incoherent mode in the upstream region, implying that it may induce convergent electron transport. The implications of both of these modes on confinement and thrust generation is discussed.

I. Nomenclature

f	=	particle distribution function
x	=	position
v	=	velocity
q	=	particle charge
m	=	particle mass
E	=	electric field
B	=	magnetic field
ν	=	collision frequency
u	=	average particle velocity
n_e	=	electron number density
ϕ	=	plasma potential
T_e	=	effective electron temperature
i	=	ion saturation current
k	=	wavenumber
ω	=	angular frequency
v_E	=	$E \times B$ drift
v_D	=	diamagnetic drift
r_L	=	electron Larmor radius
Z	=	plasma dispersion function

*AIAA Junior Member, Ph.D. Candidate, Plasmadynamics and Electric Propulsion Laboratory, Department of Aerospace Engineering, shadrach@umich.edu

†AIAA Senior Member, Assistant Professor, Plasmadynamics and Electric Propulsion Laboratory, Department of Aerospace Engineering, bjorns@umich.edu

- I = modified Bessel function of the first kind
- v_{te} = electron thermal speed
- ω_c = cyclotron frequency
- Ω = Hall parameter

II. Introduction

Magnetic nozzles (MNs) are a promising technology for long duration electric propulsion missions. Fundamentally, they consist of a diverging magnetic field applied to a plasma. As the plasma expands, a cross-field pressure gradient induces an electron diamagnetic drift that couples to the applied field to generate thrust via a $\vec{j} \times \vec{B}$ force. As these thrusters are fairly ambivalent to the ionizations scheme, they allow for contactless ionization from a radiofrequency or ionization source. This possibility removes the need for plasma-wetted electrodes, allowing for use of exotic propellants that might corrode such a surface. The ability to use more corrosive propellants enables refueling from compounds found in space, such as water [1]. Furthermore, the axial magnetic field in the ionization region mitigates plasma transport to the walls, minimizing erosion and allowing for long duration missions. Taken together, the use of magnetic nozzles will allow for extreme duration missions with the possibility for in-space refueling.

Despite their promise, MNs have yet to be operated in space. One of the factors contributing to this lack of historical use is that there are still several important open questions regarding their operation. Among these questions is that of plasma detachment. Since the applied magnetic fields will return to their origin, the plasma needs some way to separate from the field topology, otherwise it will also return to the thruster and negate any thrust it would otherwise produce. While many of these devices exhibit field strengths that are too weak to directly influence ions in this manner, electrons are often more stubborn. Since magnetic nozzles are globally current-free, the electrons must also separate from field lines for the MN to produce thrust.

Multiple theories have been proposed that allow electrons to detach. The first of these is classical resistivity [2]. The main idea of this theory is that classical collisions disrupt the electron orbits, allowing them to cross field lines. Secondly, finite electron inertia incorporated into the fluid equations has been shown to allow cross-field transport without collisions [3, 4]. As electrons orbit around centerline with a cross-field drift, their finite Larmor radius allows movements across field lines as well. The third theory is magnetic field line stretching, where the azimuthal current generates magnetic fields that stretch the background field out until the magnetic field weakens to the point of no longer affecting the electrons [5]. Finally, instabilities have been proposed to enhance resistivity to the point of inducing transport, even when classical collisions are not relevant [6, 7]. The latter theory is the focus of the current work.

Instabilities have been observed in a multitude of plasmas, ranging from small scale laboratory plasmas [8–11] to kilometer scale space plasmas [12, 13]. Of particular note in the current context is a class of instabilities that derive their energy from relative motion between electrons and ions. These drift-driven instabilities slow down electrons and manifest as an enhanced resistivity, inducing cross-field motion. This class of wave is present in many types of plasmas and often enhances transport in propulsion experiments [14–16]. While extensive interest in this field has been related to $E \times B$ discharges such as Hall thrusters, recent work has shown that unstable motion may contribute significantly to electron dynamics in magnetic nozzles as well. Namely, the influence of an incoherent lower hybrid drift instability (LHDI) has recently been observed in such a device. This presence was shown through a definition of an effective collision frequency to induce electron transport several orders of magnitude higher than classical collisions. However, this previous test was limited to a single operating condition, leaving an open question as to how prevalent this mode is under different circumstances. Furthermore, a low frequency, coherent mode has been observed in MNs as well. It has been explained as an ion acoustic instability in a helicon source [17] and has been observed as well in an electron cyclotron resonance source [7], but full observation and understanding of its dispersion is still lacking.

Given the impact that electron detachment has on the performance of an MN and the current lack of understanding regarding a prominent cross-field transport mechanism, the need is apparent to explore unstable motion in an MN plume and determine their impact on a variety of operating conditions. To this end, we organize this work as follows. In Sect. III, we discuss the general theory behind wave induced transport and introduce the concepts of convergent and divergent electron transport, focusing on how each affects thruster performance. In Sect. IV, we describe the experiment that we performed to determine the role of instabilities in a magnetic nozzle while varying the propellant flow rate. We then present the results from the experiment in Sect. V and discuss our observations in the context of electron transport in Sect. VI. Finally, we summarize our findings and discuss continuation of this work in Sect. VII.

III. Theory

The influence of instabilities on cross-field transport can be described by an effective collision frequency. This is a common approach and is often used to predict the degree of cross field transport in a wide variety of plasmas [18–21]. To elaborate on this concept mathematically, we begin with the three dimensional Vlasov equation for an arbitrary species:

$$0 = \frac{\partial f}{\partial t} + \vec{v} \frac{\partial f}{\partial \vec{x}} + \frac{q}{m} (\vec{E} + \vec{v} \times \vec{B}) \frac{\partial f}{\partial \vec{v}} \quad (1)$$

where f is the particle distribution function, \vec{E} is the electric field, \vec{v} is the particle velocity, and \vec{B} is the magnetic field. To derive the time-averaged effect that oscillations have on electron motion, we perturb n , f , and E in a sinusoidal manner assuming propagation in the \hat{x} direction as $n = n_0 + n_1$, where $n_1 = \tilde{n}_1 \exp(-i\omega t + ikx)$, with ω as the angular frequency and k the wavenumber. Keeping higher order terms and phase averaging, we obtain a Boltzmann equation with a collision term defined by the oscillating quantities [19],

$$-\frac{q}{m} \langle \tilde{E} \frac{\partial \tilde{f}}{\partial v} \rangle = \frac{\partial f}{\partial t} + \vec{v} \frac{\partial f}{\partial \vec{x}} + \frac{q}{m} (\vec{E} + \vec{v} \times \vec{B}) \frac{\partial f}{\partial \vec{v}} \quad (2)$$

where the angle brackets represent a phase average. Thus, even though no collisions are taking place, the presence of number density and electric field oscillations that are in phase can yield a drag on an electron population. The magnitude of this drag depends on the severity of the oscillations and the phase correlation between \tilde{E} and $\partial \tilde{f} / \partial t$.

To examine this effect from a fluid perspective, we may integrate Eqn. 2 in velocity space to obtain the effective collision frequency,

$$\nu_{eff} = \frac{-q \langle \tilde{n} \tilde{E} \rangle}{nm\mu} \quad (3)$$

By defining this value, we have derived a metric of the effect that unstable modes have on inducing drag on electrons. Moreover, this value can be compared directly to classical collisions [22] to determine if one dominates over the other. The definition of an effective collision frequency is a common means of determining the impact of instabilities on plasma dynamics.

The effects of instabilities on electron cross field transport has been observed in a multitude of laboratory plasmas [14, 20, 23, 24]. The specific application to magnetic nozzles is somewhat recent and may impact the device operation in unique ways. A common question regarding this impact is the direction in which they induce transport. Namely, electrons can progress *convergently* or *divergently* [3]. In the former, electrons are pulled—often by the electric field— inwards to rejoin the ions. In the convergent transport scenario, electrons progress from a more restrictive magnetic field geometry to a less restrictive one, eventually enabling escape from the system and, consequently, thrust generation. In the divergent case, electrons are typically pushed outwards by their own pressure gradient. In this situation, they move to a *more* restrictive field geometry, implying tighter field line curvature. If divergent separation is the only mechanism by which electrons cross field lines, they are never able to escape the magnetic field. They will inevitably return to the thruster, negating any axial electric field and negating thrust. Fig. 1 presents the exaggerated situations where electrons are fully divergent and fully convergent. It is necessary to note that these situations represent the extreme in each direction, whereas the reality is likely an intermediate. We have simplified this discussion by assuming that the pressure gradient is always divergent and the electric field is always convergent, whereas the reality may be somewhat more complex [4, 7, 25]. However, the typical directions of these forces can be inferred by simply observing the limits of the plume. On centerline, there is a finite and positive plasma density and pressure. Far off of centerline, these values must fall, implying that both gradients will overall be oriented generally inwards.

The relative dominance between the pressure gradient and the electric field manifests in the direction of electron drift. Namely, given that these two forces are the main factors acting on the electrons, they will each give rise to opposing drifts. An inward pressure gradient will give rise to a diamagnetic drift, while the electric field will induce a paramagnetic $\vec{E} \times \vec{B}$ current, which is usually not negated by the ions because they are not magnetized. Of course, both of these situations will reverse if the gradients change directions. These currents, in turn, directly affect thrust generation. A diamagnetic drift interacts with the radial component of \vec{B} of the applied magnetic field, inducing a $\vec{j} \times \vec{B}$ force that pushes the plasma away from the thruster. A paramagnetic drift induces an opposing force that negates thrust. As magnetic nozzles are typically diamagnetic [26–28], these currents are often favorable.

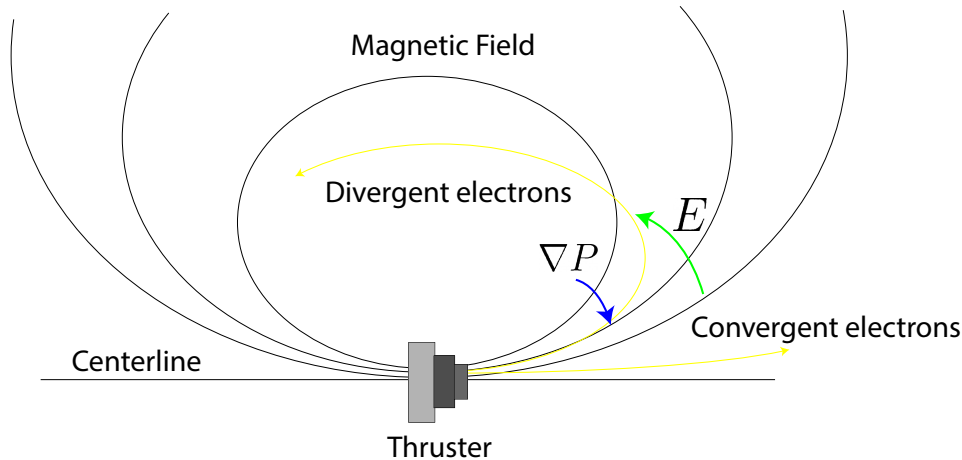


Fig. 1 Convergent and divergent transport scenarios. If the pressure gradient drives the electron motion, they will separate outwards, while if the electric field dominates, they will converge and rejoin the ions. These forces represent typical directions in magnetic nozzles and are not universal.

Resistivity, whether classical or wave-induced, modifies electron trajectories in two main ways. First, it directly decreases the azimuthal drift velocity and current. As a result, any thrust generated by a diamagnetic current or negated by a paramagnetic current will decrease. Moreover, as electrons are inhibited from orbiting, they will cross magnetic field lines. If the net drift is diamagnetic- implying generally that the pressure gradient is stronger than the electric field- electrons will likely separate divergently. While the extreme case implies returning to the thruster, even in the intermediate case diverging electrons may have a negative effect on thruster performance. Namely, as they separate from the ions farther the radial electric field will strengthen, which will cause ions to diverge as well. Indeed, since ions typically maintain little pressure of their own and are too massive to interact with the applied magnetic field, this radial electric field is the only means by which they diverge. Thus, diverging electrons induce divergence efficiency loss in thrust production. Resistivity in a paramagnetic current, on the other hand, will induce convergent transport, allowing electrons to rejoin the ions and collimate the beam, reducing divergence losses. As a result, diamagnetic and paramagnetic currents can each either harm or benefit thruster performance, depending on the level of resistivity.

The paradigm of the competing azimuthal currents is the perspective from which we approach the current work. While we are investigating the role of instabilities and the quantification of cross-field transport in the effective collision frequency, it is also vital to analyze these results with thrust generation in mind. In the ideal magnetic nozzle, a diamagnetic current would persist upstream with zero inhibition, allowing the current to maximize to interact with the applied magnetic field. As the field weakens downstream, the electron motion would change direction, and simultaneously an intense azimuthal resistivity would form, slowing down the thrust negation and allowing the electrons to rejoin the ions and collimate the beam. In this work, we perform an experiment to explore the role of instabilities in increasing resistivity and examine the results through the lens of its impact on device performance.

IV. Methods

To explore the concept of wave-induced resistivity, we performed an experiment on the PEPL electron cyclotron resonance (ECR) thruster, which inherits many design considerations from ONERA's MINOTOR [29]. We conducted these tests in the Junior vacuum facility at the University of Michigan. The thruster is composed of a microwave ionization scheme with a center-mounted antenna and a set of annular permanent magnets mounted to the back to generate the magnetic nozzle. We mounted a set of probes on three-axis motion stages, where we used the $r - z$ stages to reposition the probes and the vertical stage to switch probe sets. During this test, we operated the thruster in a floating condition with xenon as a propellant and 30W delivered to the thruster. We operated at 1 and 10 sccm-Xe as flow rates to observe the differences in wave formation with increased flow. Fig. 2 presents the overall setup of the thruster and

probes from both "front on" and "top down" perspectives.

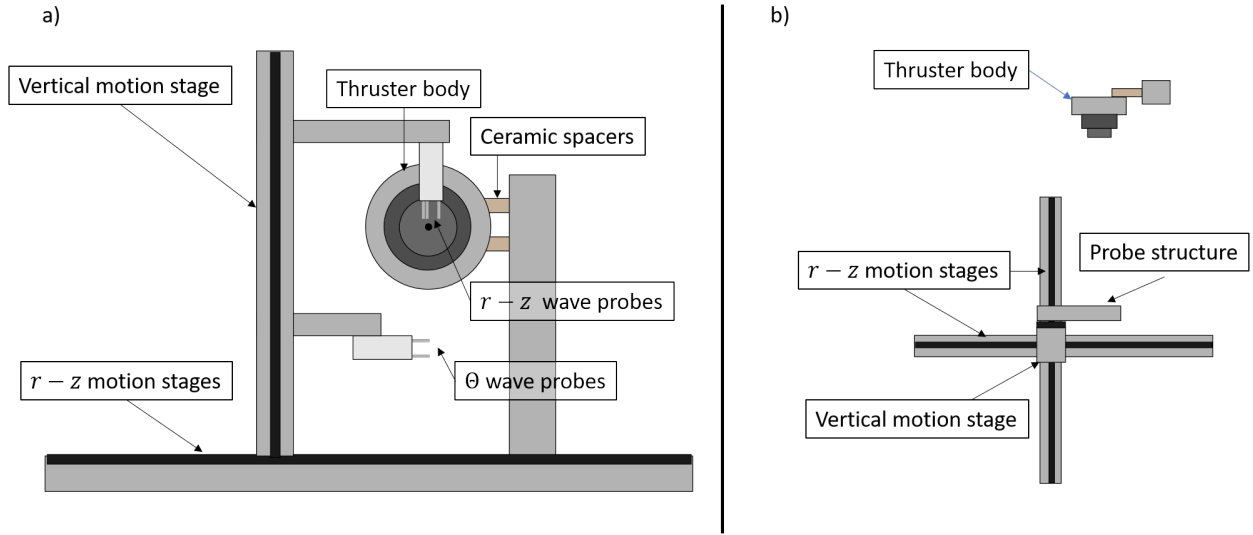


Fig. 2 Schematic of the experimental setup. a) The "front on" viewpoint. b) the "top down" view of the same setup. The five electrostatic probes are mounted in a set of three and a set of two to the vertical motion stage, which we used to change probes without breaking vacuum.

This test was composed of a Langmuir probe sweep and a wave probe test. For the Langmuir probe test, we used a signal generator and a bipolar operational amplifier to sweep the probe voltage from -110 to 110 V. Collecting the current on the probe at many voltage points and averaging across multiple sweeps led to the generation of the I-V characteristic. We followed the guidelines laid out in Ref. [30], using the Druyvesteyn method to determine the effective electron temperature and number density, and found the maximum of the first derivative of the I-V characteristic to find the plasma potential. Placing the probe on the $r-z$ motion stages allowed us to repeat this measurement throughout the plume.

To supplement the Langmuir probes, we measured the applied magnetic field with a three-axis Hall probe and Gaussmeter. We translated the probe in 5 mm increments in atmosphere to map the local magnetic field strength and direction. Doing so allowed calculation of the azimuthal electron drift velocities.

Next, we read wave presence using ion saturation probe pairs. These consisted of pairs of Langmuir probes biased to -45 V used to study wave propagation. By biasing them negatively, we can take the first-order approximation that the current drawn by each can be a relative proxy for ion number density, $i_{sat} \propto n_i$. Thus, the time-resolved measurements can tell us the magnitude of density fluctuations. We can then apply discrete Fourier analysis to convert the data into frequency space, elucidating any frequencies and turbulent characteristics that may be present in the plasma. Fig. 5 presents an example of the power spectral density (PSD) from one point in the plume at both flow conditions.

Applying this method simultaneously to two probes separated by a known distance Δx allows for evaluation of the wavenumber as well [31]. Making use of the complex component of the Fourier-transformed data, we compare the phase difference $\Delta\theta = \theta_2 - \theta_1$ at a given frequency between two probes. Assuming the wave at this frequency does not change character between the probes, the phase difference can be related to the wavenumber by $k = \Delta\theta/\Delta x$. Thus, simultaneous readings of current drawn by a pair of probes provide the wavenumber in the direction between them at each frequency.

For our purposes, we digitized measurements at a 5 MHz rate and separated our probes by 5 mm in the azimuthal direction and 7 mm in the r and z directions. We combined 100 measurements of 10 ms each to generate the intensity plots, yielding a resolution in frequency space of 500 Hz. The resulting limits in r and z are $\pm 449 \text{ m}^{-1}$, and the corresponding value in the azimuthal direction is $\pm 628 \text{ m}^{-1}$.

In this experiment, we used a total of five probes positioned on the vertical motion stage. We used three oriented downwards, separating them such that their tips formed an L in the $r-z$ plane, as indicated in Fig. 2. We took measurements from all three simultaneously, then correlated them to find propagation characteristics in the radial and axial directions. Note that we used the vertex probe as the standard Langmuir probe before taking wave measurements. After measuring waves in r and z , we repositioned the vertical stage such that the bottom set of probes was in line with

the thruster centerline. Translating these throughout the plume provided the same measurements in the vertical direction. Assuming azimuthal symmetry of the plume and aligning the probes such that their mean vertical position was in line with the thruster mid plane allowed interpreting results from this measurement as azimuthal wave propagation. Thus, through all of these measurements we are able to observe three-dimensional wave propagation throughout the plume. We also note that we performed the LP measurements and the 3D wave measurements at each condition in a single firing of the thruster at each condition, minimizing the possibility of the thruster settling into different operating modes between measurements.

V. Results

We will now discuss the direct results of these probe tests. First, we present the values derived from the Lanmguir probe sweep in Fig. 3. We must first note several qualifications to this data. First, it appears that the plasma potential of several points in the upstream region ($z \leq 70$ mm) was above the maximum value of the sweep itself. We present these values as the saturated color in Fig. 3b. Next, we observed evidence of a high energy electron population around the lower end of our sweep (-105 V). This population was seen as a slight bend in the negative end of the ion saturation region of the IV trace. For this reason, we decided to use the Druyvesteyn method to determine electron number density and did not attempt to predict ion number density, instead assuming quasineutrality in the steady state values.

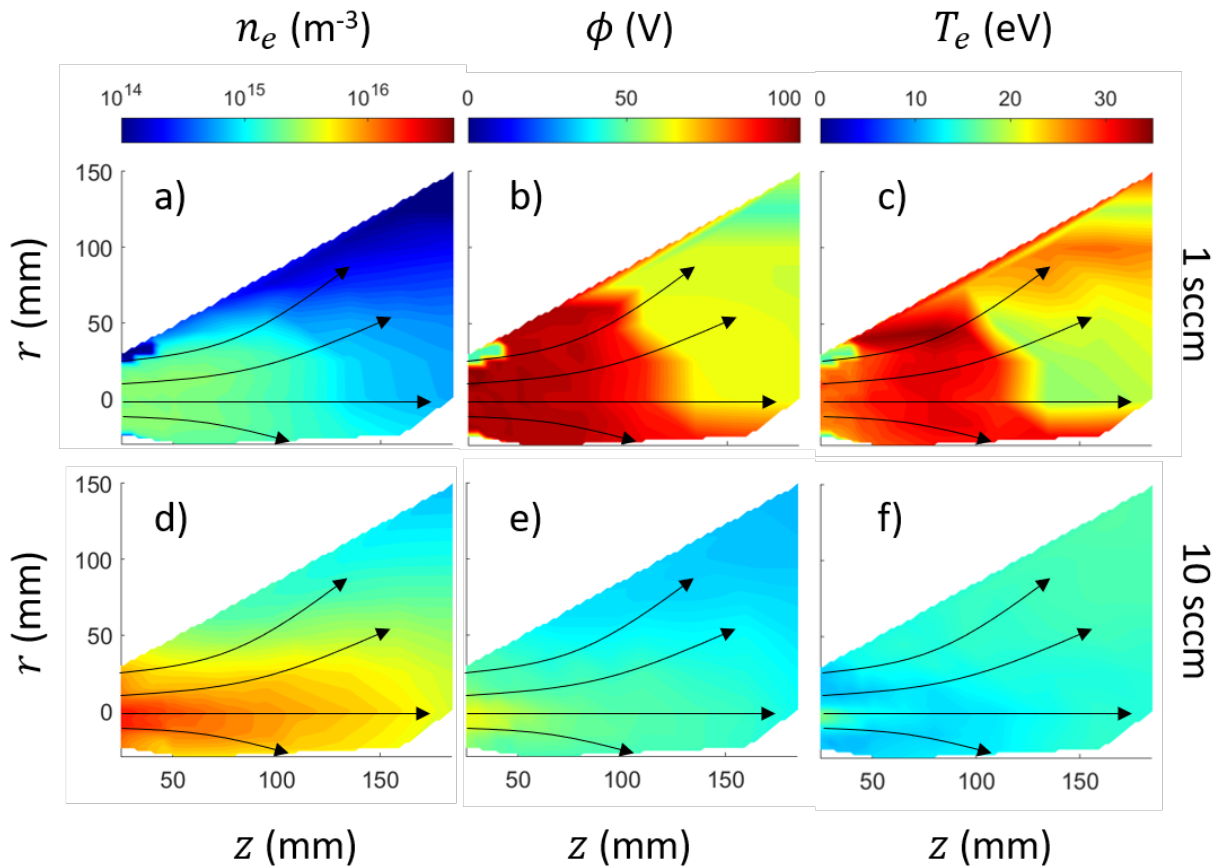


Fig. 3 Grid presenting the ion number density (a, d), plasma potential (b, e), and electron temperature (c, f) as a function of space throughout the plume for the low flow (a-c) and high flow (d-f) conditions.

Fig. 3 indicates several trends that merit discussion. First, we note that we observe significant differences with varying flow rates. Namely, the low flow rate conditions exhibit elevated electron temperatures and plasma potential. This is expected, as the plasma source is likely fully ionizing the plasma and contributing its extra energy to electron energy. As the electrons become more energized, they accelerate out of the plasma faster, inducing further charge

separation that contributes to a larger potential drop. As similarly predicted, the number density is lower in the low flow case. Higher flow rates typically yield higher number densities, as the antenna is able to deposit more energy into ionization [32].

Next, we present the results from the magnetic field measurement test. This value peaks at 300 Gauss in the plume our measurement domain and decays to only a few Gauss at 200 mm. We note that the value is likely much higher within the discharge region, as it must be to meet the electron cyclotron resonance condition at 2.4 GHz. We present the resulting map in Fig. 4.

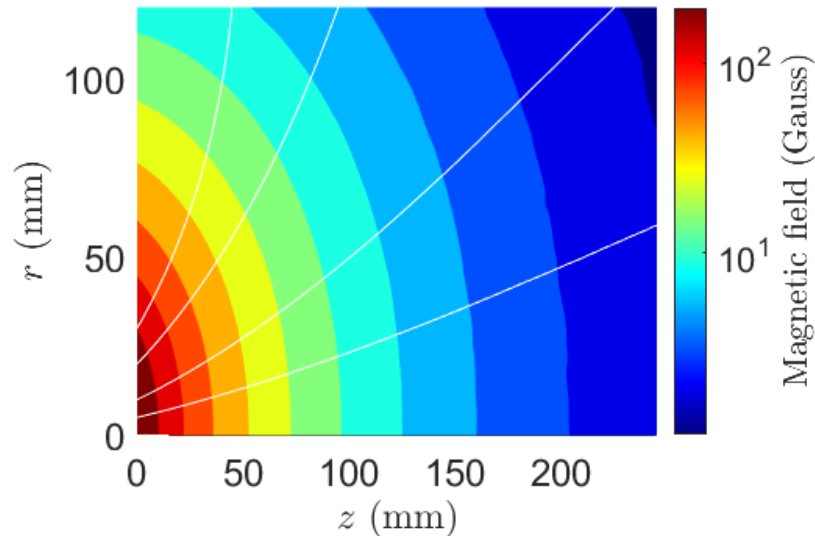


Fig. 4 Magnetic field throughout the measurement domain. White lines represent magnetic field lines.

While the Langmuir probe results offered fairly expected values, the wave probes provided measured patterns similar to what we expected, with several anomalies that merit further investigation. We will first discuss the spectral density results, an example of which we depict in Fig. 5. In the high flow condition, we observe a generally decaying spectral pattern. This pattern is reminiscent of the waves we have previously observed in this device [7]. In the low flow case, while we observe a similar decaying trend, several further interesting patterns emerge. First, a low frequency, coherent signal at 8 kHz can be seen. This type of low frequency signal has been observed previously in several magnetic nozzles, including this one [7] and the Chi Kung plasma source [17, 33]. In these previous works, it was observed at a slightly higher frequency (12 kHz), but maintained a similarly sharp and coherent pattern. The first theory to explain this wave was an ionization instability [33]; however, further tests characterizing the plasma found a lack of high energy electrons required to support such a mode [34]. The further investigation by Doyle et al. instead claims that it is an ion acoustic instability [17]. In this work, as we present in Sect. VI, we observe that this theory does not match our observations in this experiment, although it is certainly possible that the wave present in our thruster is different than in the previous works given the differences in thruster design.

Along with this low frequency mode, another significant signal appears at 150 kHz. To our knowledge, this is the first time a wave of this frequency has been observed in the plume of a magnetic nozzle, and it certainly merits further investigation. However, for the remainder of this work we focus primarily on the decaying, incoherent mode and the low frequency mode, with further investigation of the higher frequency content left to a future study.

The spectral density plots provide an idea of what content our plasma exhibits in frequency space, but to analyze dispersion we need to look to the cross-correlation between probe pairs. An example of the resulting plots in both conditions at the location $(r, z) = (45, 70)$ mm are indicated in Fig. 6. There are several factors of particular note in these plots. We first note a well-defined propagation in the azimuthal direction in both cases. This propagation is in the positive $\hat{\theta}$ condition which, according to our coordinate convention, corresponds to a diamagnetic electron drift. Typically in magnetic nozzles, the diamagnetic drift is the dominant factor in determining net electron motion,

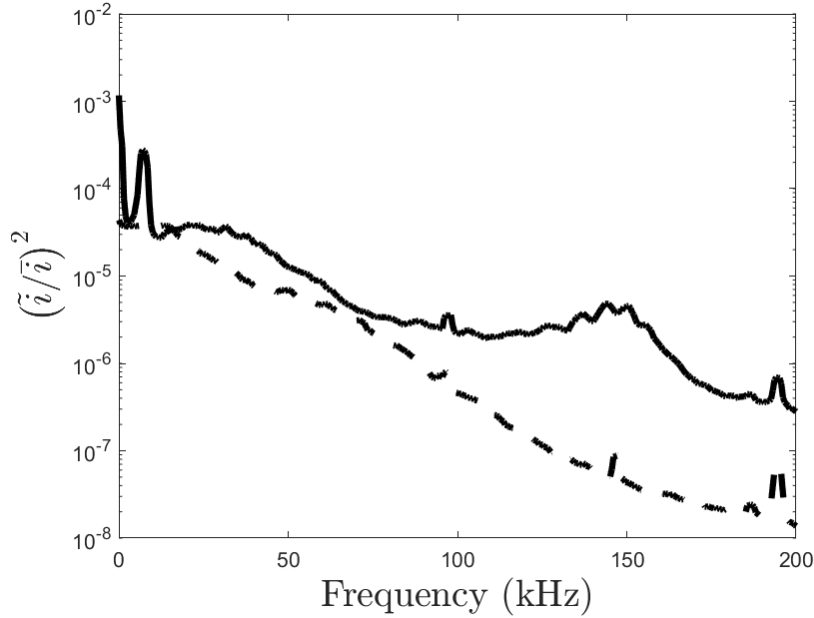


Fig. 5 Example power spectral density taken from the point $(r, z) = (45, 70)$. The solid line represents low flow, and the dashed line is high flow. The low flow reveals a sharp peak at 7 kHz and a broad peak at 146 kHz. The low frequency peak disappears at the higher flow rate, and the higher frequency signal appears far weaker.

exhibiting larger velocities than the $\vec{E} \times \vec{B}$ drift, which typically acts in the opposing direction. It is thus likely that this wave is driven by the electron drift. Furthermore, we observe a finite propagation in the $r - z$ plane as well. The low flow case exhibits small wavenumbers compared to the azimuthal direction, but the high flow seems to propagate largest in the radial direction. Finally, these patterns appear linear, to a decent approximation. The notable exceptions to this are the azimuthal wave in the low flow condition, which appears to arc downwards at higher wavenumber. The radial and axial components of the high flow case appear to arc upwards slightly as well, although the effect is somewhat less pronounced.

Taken together, we can approximate a significant propagation characteristic in the $r - z$ plane by defining k_{\parallel}/k_{θ} . This value is important to the solutions of many dispersion relations, so it is vital that we have some way to measure it. To do so, we first must estimate the phase velocity $v_{\phi} = \omega/k$ of each graph, which is indicated in Fig. 6 by red lines. We can use these phase velocities to determine the parallel propagation characteristic as

$$\frac{k_{\parallel}}{k_{\theta}} = \frac{B_r/v_{\phi_r} + B_z/v_{\phi_z}}{B} v_{\phi, \theta}. \quad (4)$$

Given local measurements of the magnetic field, we can use this value to evaluate the dispersion relation in the following section. While a more rigorous mapping of k_{θ} to k_{\parallel} would improve accuracy of this evaluation, the error on this mapping would be of a negligible magnitude given the significant width of the dispersion plots in Fig. 6. Thus, we determine the current method to be satisfactory for the purposes of this work. We present the resulting fraction in ??.

The low frequency mode maintains several interesting aspects of relevance to this work. First, it again propagates significantly in three dimensions. In the azimuthal direction, it appears to propagate downstream as an $m = 1$ azimuthal mode. However, the effective mode number decreases upstream, eventually changing directions entirely at roughly $z = 70$ mm. We present this concept in Fig. 7a, where we plot the effective mode number $m = k_{\theta}r$. There is also a significant parallel propagation, which we present in Fig. 7b. This value is necessary for evaluating the theoretical basis behind this wave.

The shift in direction that the low frequency wave exhibits is significant for two reasons. First, it likely propagates counter to the electron diamagnetic drift. Typically, the azimuthal motion of electrons in magnetic nozzle plumes is dominated by the diamagnetic drift, whereas this upstream pattern runs in a paramagnetic direction. While one might suspect that the electrons are simply paramagnetic in this region, we further note that it propagates counter to the

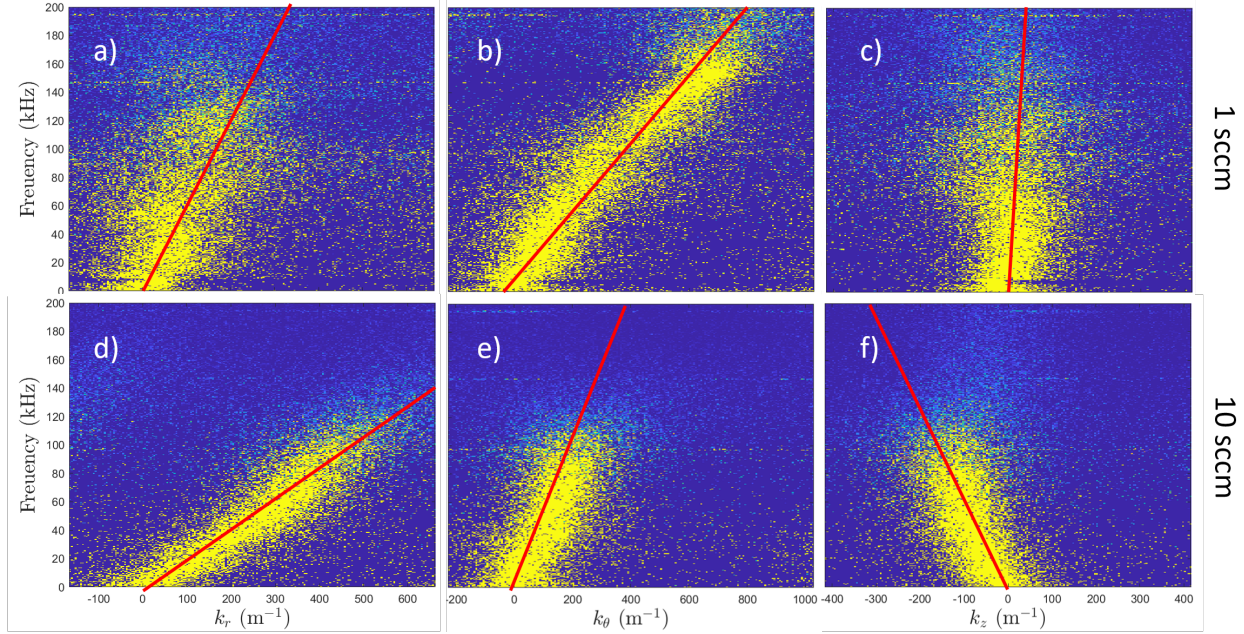


Fig. 6 Example wave intensity plots in (a, d) r , (b, e) θ , and (c, f) z taken at $(r, z) = (45, 70)$ mm at 1 sccm-Xe (a-c) and 10 sccm-Xe (d-f). Red lines indicate phase velocity estimates. Note that the radial and azimuthal plots have been adjusted for aliasing.

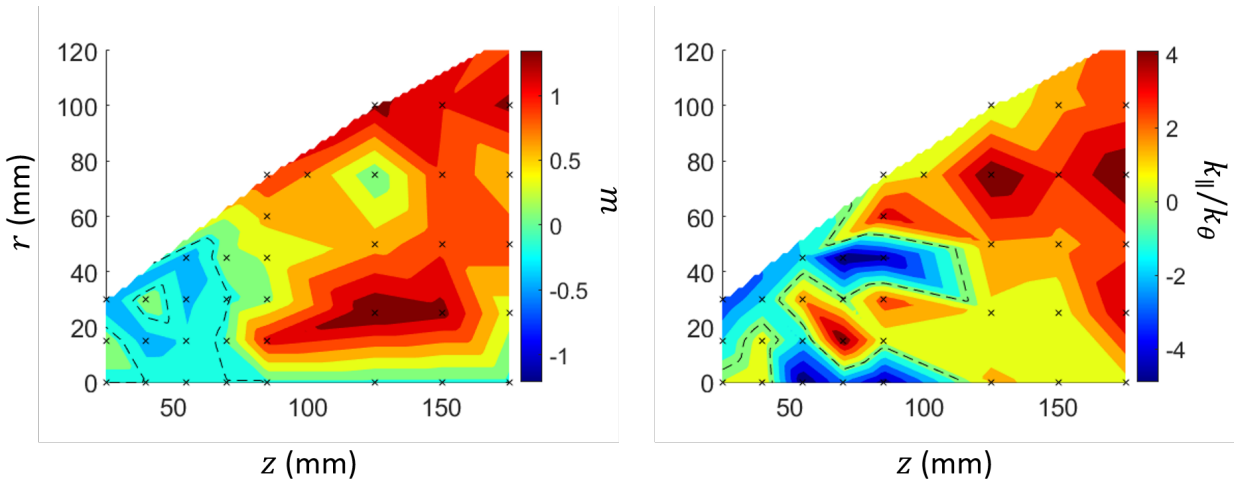


Fig. 7 Propagation characteristics of the low frequency signal, propagating at 8 ± 2 kHz. a) The azimuthal mode number, defined as $m = k_{\theta}r$, and b) the parallel propagation fraction k_{\parallel}/k_{θ} . Dashed lines represent zero, and black marks represent locations of each measurement.

incoherent mode that we observe. The incoherent mode is universally diamagnetic. This situation is illustrated in Fig. 8.

Taken together, these observations provide an opportunity for further insights into the role of instabilities in this plasma. While a full explanation of these waves merits further investigation, we proceed now to discuss several possible implications on thruster performance of these waves.

VI. Discussion

In this section, we present discussion on the impact of both the incoherent mode and the low frequency coherent mode in turn.

A. Incoherent mode

The incoherent mode observed herein has been observed in a magnetic nozzle before [7] and fits the description of a lower hybrid drift instability (LHDI). The LHDI was first theorized by Krall and Liewer [35] as an oscillation about the lower hybrid frequency that was driven unstable by an electron diamagnetic drift. It has since taken multiple forms, including the one which best describes our magnetic nozzle put forth by Carter et al. [36]. This is a kinetic wave driven unstable by a diamagnetic drift in the presence of a finite Larmor radius (as compared to the wavelength) and propagation parallel to the magnetic field. The dispersion relation is

$$0 = 1 - \frac{\omega_{pi}^2}{(\omega + k_{\perp}v_E)^2} + \frac{1}{k^2\lambda_D^2} \left[1 + \frac{\omega - k_{\theta}v_D}{k_{\parallel}v_{te}} e^{-k_{\theta}^2 r_L^2/2} I_0 \left(\frac{k_{\theta}^2 r_L^2}{2} \right) Z \left(\frac{\omega}{k_{\parallel}v_{te}} \right) \right],$$

where r_L is the electron Larmor radius, λ_D is the Debye length, and v_{te} is the electron thermal velocity. Here, Z represents the plasma dispersion function and I is a modified Bessel function of the first kind. This equation takes the form of the standard electrostatic dispersion relation with a fluid ion contribution and a kinetic electron contribution influenced by the parallel wavenumber and ratio of the Larmor radius to the wavelength.

To evaluate the LHDI's effect on electron transport, we will evaluate Eqn. 3 using the solutions to ???. To do so, we use the form of the effective collision frequency on electrons, which substitutes \tilde{E} as a function of \tilde{n} to arrive at

$$v_{eff} = \frac{v_{te}^2}{2v_D} \text{Im} \left\{ \sum_{\omega} \left(\frac{n_1(\omega)}{n} \right)^2 k \left[1 + (\omega - k_{\perp}v_D) \times \frac{1}{k_{\parallel}v_{te}} Z \left(\frac{\omega}{k_{\parallel}v_{te}} \right) e^{-(kr_L)^2/2} I_0((kr_L)^2/2) \right]^{-1} \right\}. \quad (5)$$

Here, the summation is over frequency, and $n_1(\omega)$ is the number density oscillation magnitude at each frequency. Now that we have arrived at a quantification for effective collision frequency, we may determine its effect throughout the

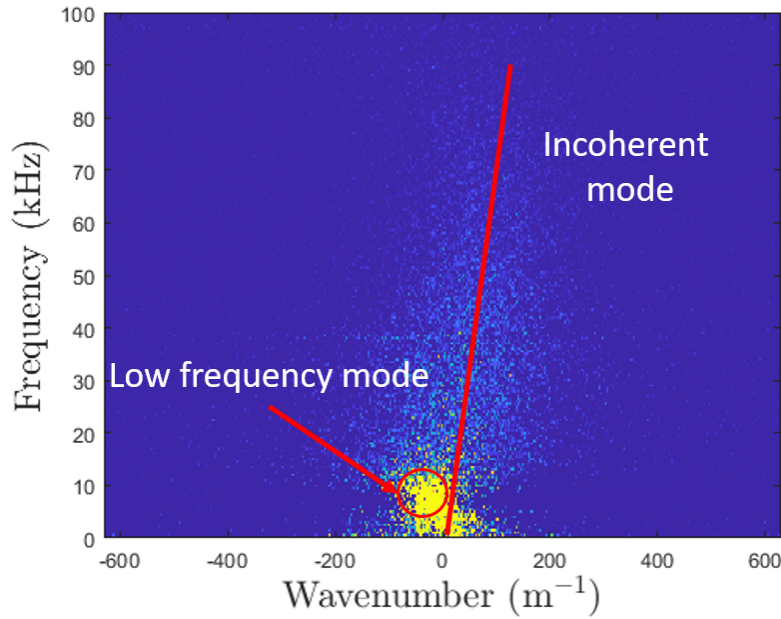


Fig. 8 Example azimuthal Beall plot taken at $(r, z) = (15, 45)$ mm. The low frequency, high intensity mode can be seen at 8 kHz propagating with negative wavenumber while the higher frequency, incoherent mode is propagating in the opposite direction.

plume for both flow conditions. To do so, we will present the data in terms of a Hall parameter, $\Omega = \frac{\omega_c}{v_{eff}}$, where $\omega_c = eB/m_e$ is the electron cyclotron frequency. We present this value for both operating conditions in Fig. 9.

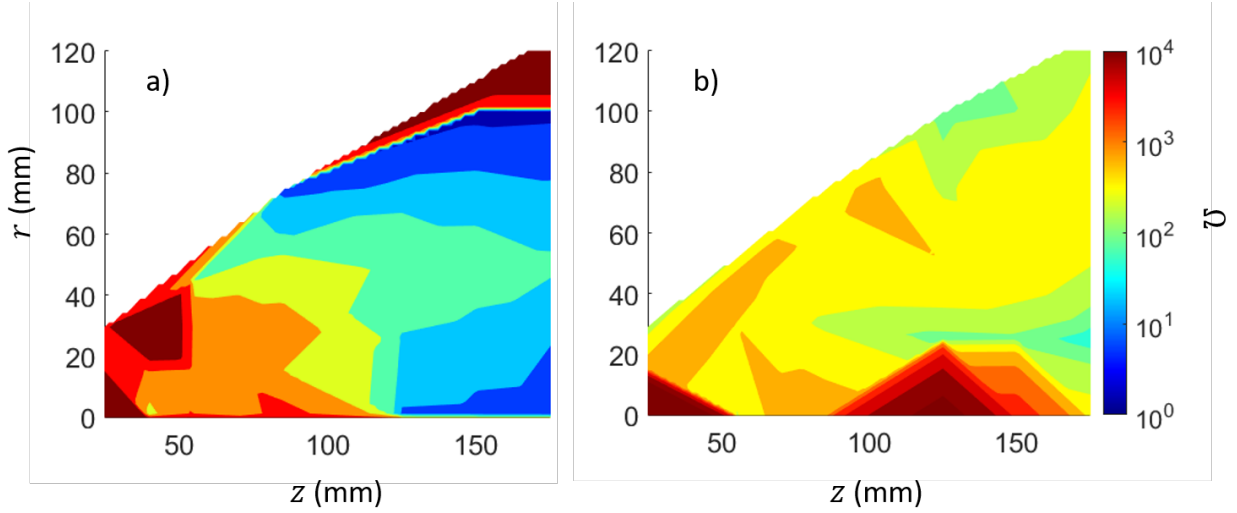


Fig. 9 Hall parameter induced by the LHDI for the a) low and b) high flow conditions.

One significant trend immediately emerges in this data. Namely, the low flow condition maintains a lower hall parameter than the high flow condition, particularly in the downstream region. For the low flow case, the hall parameter reaches the order of 10. The high flow case, while still influenced by the LHDI, reaches a hall parameter of several hundred downstream. These values have been reported in previous work to imply significant cross field transport on other devices [9], implying that in both cases enhanced transport is likely significant. The difference between the two cases, however, is still substantial. The root cause of this discrepancy is in the fact that the oscillation magnitude is smaller in the high flow case. While the cause for this is not immediately clear from the dispersion relation, we can make an educated guess from historical wave damping mechanisms. Namely, classical collisions with neutrals have been shown in the past to damp plasma oscillations [23]. While the low flow rate condition is nearly collisionless due to its low number density and high electron temperature, the high flow rate case maintains classical Coulomb collision frequencies on the order of 10^4 s^{-1} . The dispersion relation that we use to describe these waves does not allow for classical collisions- a new equation must be derived to evaluate this theory. A second, more observable theory is that the low flow case is able to contribute more energy to the wave from the elevated electron temperature. The LHDI is driven by the electron diamagnetic drift, which scales linearly with electron temperature. Given the factor of around 3 increase in T_e in the low flow condition, it is quite likely that this contribution is more significant with less flow.

B. Coherent mode

Before discussing the actual impact of these waves on electron trajectories, we will first discuss the low frequency mode. While we cannot confidently describe this wave fully at this time, we will attempt to do so for part of the plume for the sake of estimating its likely impact on electron transport. We would first like to mention that, contrary to the previous work discussing a similar mode in a magnetic nozzle, this wave is unlikely to be an acoustic mode. The simple reason for this is that the phase velocity $v_\phi = \omega/k_\parallel$ is not equal to the ion acoustic speed, $c_s = \sqrt{T_e/m_i}$. Throughout most of the plume, the parallel phase velocity barely reaches over 1 km/s, whereas the ion acoustic speed in the low flow case (where this wave appears) is around 5 km/s. Furthermore, we observe a clear azimuthal character, which does not appear in parallel ion acoustic waves [23]. Thus, it is unlikely that this low frequency mode is an ion acoustic wave.

The theory that we propose here is that this is a form of anti drift instability (ADI) driven unstable by propagation parallel to the magnetic field and electron collisions. We have previously identified a wave seen in a different magnetic nozzle as an ADI [37], and they have been observed in similar expanding field configurations [23, 38]. An azimuthally propagating ADI in these cases manifests as an $m = 1$ mode, which corresponds closely to the feature we see at around

$z = 150$ mm in Fig. 7. To describe this particular wave, we adopt the following dispersion relation [21, 39, 40]:

$$0 = -\frac{\left(\frac{m}{R}\right) v^* + i\nu_{pl}}{\omega + i\nu_{pl}} + \frac{T_e}{m_i} \left(\frac{k^2}{\omega^2}\right) \quad (6)$$

where $\nu_{pl} = k_z^2 T_e / m_e / \nu_e$. This form of the ADI requires both a finite propagation parallel to the magnetic field and a significant background electron collision frequency. While we observe parallel propagation, we note that the classical collision frequency in the low flow case is insufficient to drive this ADI unstable. However, the theory behind the ADI does not restrict what kind of resistivity must be present. We thus propose here that the ADI is driven unstable by the resistivity induced by the LHDI. This concept explains several of our observations. First, given that the effective collision frequency from the LHDI is much lower in the high flow case, it makes sense that the ADI may not be driven unstable, thus we do not expect to see this low frequency mode appear. Furthermore, incorporating effective collisions from the LHDI into the ADI dispersion relation for points in the low flow case predict real frequencies rather close to what we observe. To evaluate the dispersion relation, we incorporate the measured k_z and k_r , projecting them onto the local magnetic field unit vector to find k_{\parallel} . We also use the measured k_{θ} and solve for the real component of the frequency. Doing so consistently yields growth rates above 10 kHz, which is likely enough to form an observable wave.

Finally, again implementing Eqn. 3, we can find the anomalous collision frequency as

$$\nu_{eff} = \nu_e \left[\sum_{\omega} \left(\frac{\delta n_{\omega}}{n} \right)^2 \left(\frac{k_{\theta}}{k_{\parallel}} \right)^2 \right] \quad (7)$$

where we have used Eqn. 8 from Ref. [21] and assumed that $u_{\parallel} \ll u_{\theta}$, as is probable for electrons in magnetic nozzles due to the restriction that there is no global current [3]. Finally, applying similar analysis as we did with the LHDI, we can define the effective Hall parameter, which we present in Fig. 10.

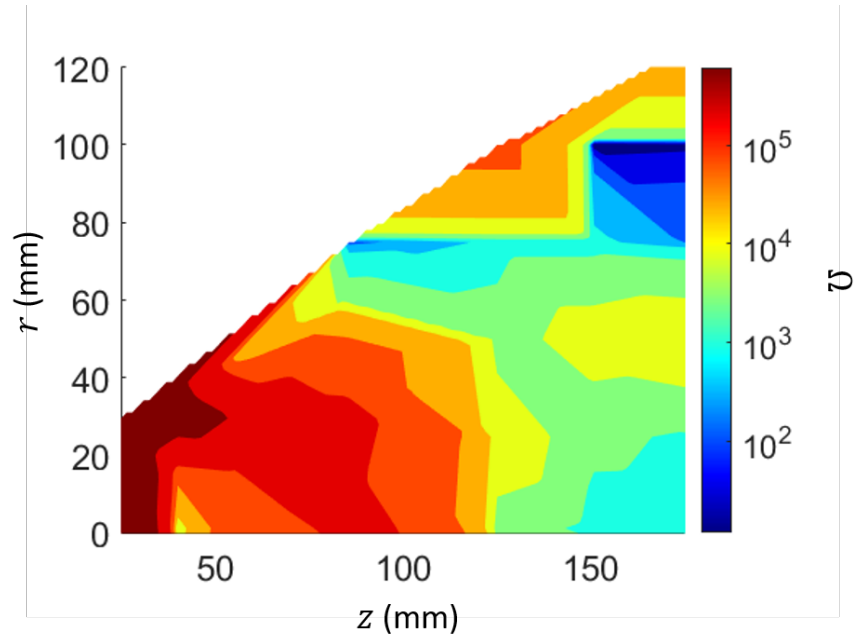


Fig. 10 Hall parameter for the low flow case induced by anomalous transport from the ADI. Note that we have changed the color scaling on this plot to visualize spatial trends.

From Fig. 10, we see that the hall parameter induced by the ADI is generally significantly higher than that induced by the LHDI. The primary reason for this is that this wave, while strong, exists only over a very narrow frequency range with a width of around 500 Hz. It is generally weakest upstream, but increases in strength with the LHDI downstream. However, based on this theory, it appears that it is not dominant anywhere.

C. Impact on electron transport

We are now ready to discuss the impact of these waves on thruster performance. As we described in section III, the direction of electron transport is of great relevance to the performance of a thruster. In this study, we have observed that the LHDI appears to propagate in the diamagnetic direction throughout the plume. A drag induced in this motion will thus induce divergent transport. As noted previously, this type of motion is likely to be harmful to thruster performance.

However, the comparison of the impact of these waves between flow conditions elucidates a trend in this transport that may be counter intuitive. Specifically, the high flow case seems to be affected less by this wave. Classically, a higher flow rate is likely to enhance resistive transport. The combination of increased neutral presence, increased ion density, and lower electron temperature imply an enhanced classical diffusion rate. However, according to this study, it seems more likely that the high flow plasma remains attached to field lines for longer given the decrease in wave-induced transport.

The low frequency mode appears to influence the plasma in a different way. While it follows the LHDI throughout most of the plume, in the upstream region it seems to propagate in the opposite direction. By propagating in the direction of a paramagnetic electron drift, it appears that the effect of this wave would be to converge electrons. The presence of this wave upstream, however, likely does very little for eventual electron convergence.

VII. Conclusions

In this work, we have observed a pair of unstable modes throughout the plume of a magnetic nozzle. The first is an incoherent mode that propagates in the direction of a diamagnetic electron drift which we identified as a lower hybrid drift instability. Applying quasilinear theory to determine an effective hall parameter, we see that the induced drag is likely able to allow electrons to separate from magnetic field lines. This effect is much more pronounced in the lower flow condition than in the higher. Since it propagates in the diamagnetic direction, the induced drag will induce divergent transport, likely enhancing the radial electric field and diverging the plume.

In the same experiment, we observed a low frequency mode as well. While higher amplitude, this wave is likely less significant than the LHDI because of its narrow spectral presence. However, it exhibits the interesting property of propagating in the paramagnetic direction upstream, which would convergent transport. Downstream, it changes direction and propagates with the LHDI, contributing slightly to further divergence. This mode also does not appear at all in the high flow case.

These observations have prompted several questions for further study. Namely, we would like to further solidify the theory behind the low frequency mode. While the ADI is a possibility for the downstream region, the transition to a mode number less than one and eventual change of direction do not fit this theory well. Moreover, we have observed another coherent mode at around 150 kHz. We have not attempted in this work to theoretically describe this mode, nor have we quantified its impact on electron transport. This mode might be significant in the question of electron transport, and only in describing it as well will we be able to develop a cohesive picture of instability-induced transport in magnetic nozzles.

VIII. Acknowledgements

This work was funded by the NASA Space Technology and Research Fellowship grand number 80NSSC17K0156. We would like to thank all members of the Plasmadynamics and Electric Propulsion Laboratory for the insightful conversations and experimental support.

References

- [1] Sheppard, A. J., and Little, J. M., "Theoretical scaling laws for water-vapor propellant thrusters," *International Electric Propulsion Conference2*, Vienna, 2019.
- [2] Moses, R. W., Gerwin, R. A., and Schoenberg, K. F., "Resistive plasma detachment in nozzle based coaxial thrusters," *Proc. 9th Symp. Space Nucl. Power Syst. AIP Conf.*, Vol. 246, 1992, pp. 1293–1303. URL <https://doi.org/10.1063/1.41752><http://aip.scitation.org/toc/apc/246/1>.
- [3] Ahedo, E., and Merino, M., "Two-dimensional plasma expansion in a magnetic nozzle: Separation due to electron inertia," *Phys. Plasmas*, Vol. 19, No. 083501, 2012, p. 43504. <https://doi.org/10.1063/1.4739791>, URL <http://aip.scitation.org/toc/php/19/8>.
- [4] Little, J. M., and Choueiri, E. Y., "Electron demagnetization in a magnetically expanding plasma," *Phys. Rev. Lett.*, Vol. 123, 2019, p. 145001. <https://doi.org/10.1103/PhysRevLett.123.145001>.

- [5] Arefiev, A. V., and Breizman, B. N., “Magnetohydrodynamic scenario of plasma detachment in a magnetic nozzle,” *Phys. Plasmas*, Vol. 12, No. 043504, 2005. URL <http://aip.scitation.org/toc/php/12/4>.
- [6] Olsen, C. S., “Experimental Characterization of Plasma Detachment from Magnetic Nozzles,” Ph.D. thesis, Rice University, 2013.
- [7] Hepner, S., Wachs, B., and Jorns, B., “Wave-driven non-classical electron transport in a low temperature magnetically expanding plasma,” *Appl. Phys. Lett.*, Vol. 116, No. 263502, 2020. <https://doi.org/10.1063/5.0012668>.
- [8] Fenneman, D. B., Raether, M., and Yamada, M., “Ion-acoustic instability in the positive column of a helium discharge,” *Phys. Fluids*, Vol. 16, No. 6, 1973, p. 871. <https://doi.org/10.1063/1.1694439>.
- [9] Boeuf, J. P., and Garrigues, L., “ $E \times B$ electron drift instability in Hall thrusters: Particle-in-cell simulations vs. theory,” *Phys. Plasmas*, Vol. 25, No. 061204, 2018. <https://doi.org/10.1063/1.5017033>.
- [10] Georgin, M. P., Jorns, B. A., and Gallimore, A. D., “Correlation of ion acoustic turbulence with self-organization in a low-temperature plasma,” *Phys. Plasmas*, Vol. 26, No. 82308, 2019. <https://doi.org/10.1063/1.5111552>.
- [11] Lafleur, T., Martorelli, R., Chabert, P., and Bourdon, A., “Anomalous electron transport in Hall-effect thrusters: Comparison between quasilinear kinetic theory and particle-in-cell simulations,” *Phys. Plasmas*, Vol. 25, No. 061202, 2018, p. 61202. <https://doi.org/10.1063/1.5017626>.
- [12] Roytershteyn, V., Daughton, W., Karimabadi, H., and Mozer, F. S., “Influence of the Lower-Hybrid Drift Instability on Magnetic Reconnection in Asymmetric Configurations,” *Phys. Rev. Lett.*, Vol. 108, No. 185001, 2012. <https://doi.org/10.1103/PhysRevLett.108.185001>.
- [13] Norgren, C., Vaivads, A., Khotyaintsev, Y. V., and André, M., “Lower Hybrid Drift Waves: Space Observations,” *Phys. Rev. Lett.*, Vol. 109, No. 055001, 2012. <https://doi.org/10.1103/PhysRevLett.109.055001>.
- [14] Cavalier, J., Lemoine, N., Bonhomme, G., Tsikata, S., Honoré, C., Grésillon, D., Honor, C., and Gr Esillon, D., “Hall thruster plasma fluctuations identified as the electron drift instability: Modeling and fitting on experimental data,” *Phys. Plasmas*, Vol. 20, No. 082107, 2013. <https://doi.org/10.1063/1.4817743>.
- [15] Ducrocq, A., Adam, J. C., Héron, A., and Laval, G., “High-frequency electron drift instability in the cross-field configuration of Hall thrusters,” *Phys. Plasmas*, Vol. 13, No. 102111, 2006. <https://doi.org/10.1063/1.2359718>.
- [16] McDonald, M. S., and Gallimore, A. D., “Rotating spoke instabilities in Hall thrusters,” *IEEE T Plasma Sci.*, Vol. 39, No. 11, 2011, pp. 2952–2953.
- [17] Doyle, S. J., Bennet, A., Tsifakis, D., Dedrick, J. P., Boswell, R. W., and Charles, C., “Characterization and Control of an Ion-Acoustic Plasma Instability Downstream of a Diverging Magnetic Nozzle,” *Front. Phys.*, Vol. 8, No. 24, 2020. <https://doi.org/10.3389/fphy.2020.00024>, URL <http://eprints.whiterose.ac.uk/157405/>.
- [18] Sagdeev, R. Z., “Critical problems in plasma astrophysics. I. Turbulence and nonlinear waves,” Tech. rep., Space Research Institute, Moscow, U.S.S.R., 1979. URL <https://journals.aps.org/rmp/pdf/10.1103/RevModPhys.51.1>.
- [19] Davidson, R. C., and Gladd, N. T., “Anomalous transport properties associated with the lower-hybrid-drift instability,” *Phys. Fluids*, Vol. 18, No. 1327, 1975. <https://doi.org/10.1063/1.861021>, URL <https://aip.scitation.org/toc/pfl/18/10>.
- [20] Brown, Z. A., and Jorns, B. A., “Spatial evolution of small wavelength fluctuations in a Hall Thruster,” *Physics of Plasmas*, Vol. 26, No. 11, 2019, p. 113504. <https://doi.org/10.1063/1.5116708>, URL <http://aip.scitation.org/doi/10.1063/1.5116708>.
- [21] Jorns, B. A., Cusson, S. E., Brown, Z., and Dale, E., “Non-classical electron transport in the cathode plume of a Hall effect thruster,” *Physics of Plasmas*, Vol. 27, No. 2, 2020, p. 022311. <https://doi.org/10.1063/1.5130680>, URL <http://aip.scitation.org/doi/10.1063/1.5130680>.
- [22] Spitzer, L., and Haem, R., “Transport phenomena in a completely ionized gas,” *Phys. Rev.*, Vol. 89, No. 5, 1953, pp. 977–981. URL <https://journals.aps.org/pr/pdf/10.1103/PhysRev.89.977>.
- [23] Jorns, B. A., Mikellides, I. G., and Goebel, D. M., “Ion acoustic turbulence in a 100-A LaB6 hollow cathode,” *Phys. Rev. E.*, Vol. 90, No. 6, 2014, pp. 1–10. <https://doi.org/10.1103/PhysRevE.90.063106>.
- [24] Tsikata, S., and Minea, T., “Modulated Electron Cyclotron Drift Instability in a High-Power Pulsed Magnetron Discharge,” *Phys. Rev. Lett.*, Vol. 114, No. 185001, 2015. <https://doi.org/10.1103/PhysRevLett.114.185001>, URL <https://journals.aps.org/prl/pdf/10.1103/PhysRevLett.114.185001>.

- [25] Collard, T. A., and Jorns, B. A., "Magnetic nozzle efficiency in a low power inductive plasma source," *Plasma Sources Sci. Technol.*, Vol. 28, No. 105019, 2019. <https://doi.org/10.1088/1361-6595/ab2d7d>.
- [26] Ahedo, E., and Merino, M., "Two-dimensional supersonic plasma acceleration in a magnetic nozzle," *Phys. Plasmas*, Vol. 17, No. 17, 2010, p. 7. URL <http://aip.scitation.org/toc/php/17/7>.
- [27] Roberson, B. R., Winglee, R., and Prager, J., "Enhanced diamagnetic perturbations and electric currents observed downstream of the high power helicon," *Phys. Plasmas*, Vol. 18, No. 053505, 2011. <https://doi.org/10.1063/1.3574753>, URL <http://earthweb.ess.washington.edu/winglee/RecentPapers/2011HighPowerHelicon.pdf>.
- [28] Takahashi, K., Akahoshi, H., Charles, C., Boswell, R. W., and Ando, A., "High Temperature Electrons Exhausted from rf Plasma Sources Along a Magnetic Nozzle," *Phys. Plasmas*, Vol. 24, No. 084503, 2017. <https://doi.org/10.1063/1.4990110>, URL <http://aip.scitation.org/toc/php/24/8>.
- [29] Vialis, T., and Jarrige, J., "Direct thrust measurement of an electron cyclotron resonance plasma thruster," *J Propul Power*, Vol. 34, No. 5, 2018. <https://doi.org/10.2514/1.B37036>.
- [30] Sheehan, J. P., Raitzes, Y., Hershkowitz, N., and McDonald, M., "Recommended Practice for Use of Emissive Probes in Electric Propulsion Testing," *J Propul Power*, Vol. 33, No. 3, 2017, pp. 614–637. <https://doi.org/10.2514/1.B35697>, URL <https://arc.aiaa.org/doi/10.2514/1.B35697>.
- [31] Beall, J. M., Kim, Y. C., and Powers, E. J., "Estimation of wavenumber and frequency spectra using fixed probe pairs," *J. Appl. Phys.*, Vol. 53, No. 6, 1982. <https://doi.org/10.1063/1.331279>.
- [32] Geller, R., *Electron Cyclotron Resonance Ion Sources and ECR Plasmas*, United Kingdom: Institute of Physics, 1996.
- [33] Aanesland, A., Charles, C., Lieberman, M. A., and Boswell, R. W., "Upstream Ionization Instability Associated with a Current-Free Double Layer," *Phys. Rev. Lett.*, Vol. 97, No. 075003, 2006. <https://doi.org/10.1103/PhysRevLett.97.075003>.
- [34] Takahashi, K., Charles, C., Boswell, R., and Hatakeyama, R., "Radial characterization of the electron energy distribution in a helicon source terminated by a double layer," *Phys. Plasmas*, Vol. 15, No. 074505, 2008. <https://doi.org/10.1063/1.2959137>.
- [35] Krall, N. A., and Liewer, P. C., "Low-Frequency Instabilities in Magnetic Pulses," *Phys. Rev. Lett.*, Vol. 4, No. 5, 1971. URL <https://journals.aps.org/prl/pdf/10.1103/PhysRevLett.4.2094>.
- [36] Carter, T. A., Yamada, M., Ji, H., Kulsrud, R. M., and Trintchouk, F., "Experimental study of lower-hybrid drift turbulence in a reconnecting current sheet," *Phys. Plasmas*, Vol. 9, No. 8, 2002, p. 3272. <https://doi.org/10.1063/1.1494433>.
- [37] Hepner, S., Collard, T., Little, J., and Jorns, B., "Low-Frequency Plasma Oscillations in the Plume of a Low Temperature Magnetic Nozzle," *International Electric Propulsion Conference*, 2017-515, atlanta, GA, 2017. URL https://iepc2017.org/sites/default/files/speaker-papers/iepc_2017_10_30.pdf.
- [38] Light, M., Chen, F. F., and Colestock, P. L., "Low frequency electrostatic instability in a helicon plasma," *Phys. Plasmas*, Vol. 8, No. 10, 2001. <https://doi.org/10.1063/1.1403415>.
- [39] Frias, W., Smolyakov, A. I., Kaganovich, I. D., and Raitzes, Y., "Long Wavelength Gradient Drift Instability in Hall Plasma Devices. I. Fluid Theory," *Physics of Plasmas II. Applications Physics of Plasmas Journal of Applied Physics*, Vol. 19, No. 8, 2012, pp. 72112–52108. <https://doi.org/10.1063/1.4736997>, URL <http://aip.scitation.org/toc/php/19/7>.
- [40] Sakawa, Y., Joshi, C., Kaw, P. K., Chen, F. F., and Jain, V. K., "Excitation of the Modified Simon Hoh Instability in an Electron Beam Produced Plasma," *Physics of Fluids B: Plasma Physics*, Vol. 5, No. 6, 1993. <https://doi.org/10.1063/1.4972269>, URL <http://aip.scitation.org/toc/pfb/5/6>.